Received: 23 March 2018 | Revised: 30 August 2018 | Accepted: 5 September 2018

DOI: 10.1111/cns.13069

ORIGINAL ARTICLE

WILEY CNS Neuroscience & Therapeutics Open Access

Inhibition of ferroptosis attenuates tissue damage and improves long-term outcomes after traumatic brain injury in mice

Bao-Shu Xie[1,2] | Yi-Qin Wang[3] | Yong Lin[1,2] | Qing Mao[1] | Jun-Feng Feng[1,2] | Guo-Yi Gao[1,2] | Ji-Yao Jiang[1,2]

[1]Department of Neurosurgery, School of Medicine, Ren Ji Hospital, Shanghai Jiao Tong University, Shanghai, China

[2]Shanghai Institute of Head Trauma, Shanghai, China

[3]Sino-French Research Center for Life Sciences and Genomics, State Key Laboratory of Medical Genomics, Rui-Jin Hospital, Shanghai Jiao Tong University School of Medicine, Shanghai, China

Correspondence
Guo-Yi Gao, Department of Neurosurgery, Ren Ji Hospital, School of Medicine, Shanghai Jiao Tong University, Pudong New District, Shanghai, China.
Email: gao3@sina.com
and
Ji-Yao Jiang, Department of Neurosurgery, Ren Ji Hospital, School of Medicine, Shanghai Jiao Tong University, Pudong New District, Shanghai, China.
Email: jiyaojiang@126.com

Funding information
Doctoral Innovation Fund Projects from Shanghai Jiao Tong University School of Medicine, Grant/Award Number: BXJ201824; National Natural Science Foundation of China, Grant/Award Number: No.81772058, 81471856 and 81471244 and 81771317

Summary

Aims: Ferroptosis, a new form of iron-dependent programmed cell death, has been shown to be involved in a range of diseases. However, the role of ferroptosis in traumatic brain injury (TBI) has yet to be elucidated. We aimed to investigate whether ferroptosis is induced after TBI and whether the inhibition of ferroptosis would protect against traumatic brain injury in a controlled cortical impact injury (CCI) mouse model.

Methods: After establishing the TBI model in mice, we determined the biochemical and morphological changes associated with ferroptosis, including iron accumulation with Perl's staining, neuronal cell death with Fluoro-Jade B (FJB) staining, iron metabolism dysfunction with Western blotting, reactive oxygen species (ROS) accumulation with malondialdehyde (MDA) assays, and shrunken mitochondria with transmission electron microscopy. Furthermore, a specific inhibitor of ferroptosis, ferrostatin-1(fer-1), was administrated by cerebral ventricular injection after CCI. We used cresyl violet (CV) staining to assess lesion volume, along with the Morris water maze and beam walk test to evaluate long-term outcomes.

Results: TBI was followed by iron accumulation, dysfunctional iron metabolism, the upregulation of ferroptosis-related genes, reduced glutathione peroxidase (GPx) activity, and the accumulation of lipid-reactive oxygen species (ROS). Three days (d) after TBI, transmission electron microscopy (TEM) confirmed that the mitochondria had shrunk a typical characteristic of ferroptosis. Importantly, the administration of Fer-1 by cerebral ventricular injection significantly reduced iron deposition and neuronal degeneration while attenuating injury lesions and improving long-term motor and cognitive function.

Conclusion: This study demonstrated an effective method with which to treat TBI by targeting ferroptosis.

KEYWORDS

ferroptosis, iron accumulation, lipid ROS accumulation, traumatic brain injury (TBI)

The first two authors contributed equally to this work.

1 | INTRODUCTION

While traumatic brain injury (TBI) is a leading cause of global mortality and morbidity worldwide, there is no effective pharmaceutical intervention for this type of condition.[1-3] Once brain impact occurs, the brain typically endures two waves of injury. Caused by mechanical damage, the primary injury usually leads to brain abnormalities in brain structure and dysfunction of the blood vessels, thus resulting in necrosis and intracranial hemorrhage. The second injury involves a complex cascade of cell death, edema, oxidative stress, iron accumulation, endoplasmic reticulum stress, inflammation, and immune response.[4-6] It is well accepted that various forms of cell death occur during the pathophysiological process which occurs after TBI, including necrosis, apoptosis, necroptosis, and pyroptosis.[7-9] Unlike animal models of TBI, which can benefit from the inhibition of apoptosis, necroptosis, and pyroptosis, there have been no reports of the successful use of cell death inhibitors in the treatment of human TBI patients. These facts suggest that a combination of these forms of cell death may play a more important role in brain tissue damage and that another form of cell death might exist and act following TBI in humans.

Ferroptosis, an iron- and reactive oxygen species (ROS)-dependent form of regulated cell death (RCD), has been reported to be involved in a variety of diseases, such as cancer, intracerebral hemorrhage, ischemia stroke, cold damage, and kidney degeneration.[10-15] This type of iron-dependent cell death is remarkably distinguishable from other forms of RCD, including apoptosis, unregulated necrosis, and necroptosis in terms of morphology, biochemistry, and genetics. The initiation of ferroptosis is not dependent on caspase-3 (a mediator of apoptosis), RIP1 or RIP3 (mediators of necroptosis), or caspase-1 or caspase-11 (mediators of pyroptosis). Rather, it is triggered by specific inducers, such as erastin and RSL3, characterized by the accumulation of intracellular iron and lipid ROS, and distinguished morphologically by the existence of shrunken mitochondria and regulated by a distinct set of genes, including RPL8, IREB2, ATP5G3, TTC35, CS, ACSF2, GPX4, ACSL4, and SLC7A11.[10,16] Moreover, this form of cell death can be specific inhibited by ferrostatin-1 and liproxstatin-1.[10,17]

Recent studies have reported that ferroptosis plays an important role in the pathophysiological process of intracerebral hemorrhage (ICH) and that inhibition of ferroptosis with ferrostatin-1 attenuates hemorrhagic brain damage in mouse models of ICH.[12,18] Interestingly, targeting ferroptosis in animal models of ischemic stroke with liproxstatin-1 attenuated the decline in motor function, progressive neurological deficits, final infarct volumes, and cognitive function.[13] A previous study, using a rat model of controlled cortical impact injury (CCI), showed that TBI was associated with significantly elevated levels of 15-HpETE-PE and 15LO2 in the brain cortex and hippocampus and a downregulation of GPX4 soon after CCI in pediatric rats. This strongly suggested the involvement of ferroptotic death after TBI.[19]

However, the precise mechanisms underlying ferroptosis in TBI and whether the inhibition of ferroptosis might protect the injured brain after TBI remain unknown. In the present study, we set out to confirm the occurrence of ferroptosis in TBI by investigating iron and lipid ROS accumulation, and by examining ultrastructural changes of the mitochondria after TBI. Furthermore, we tested the efficacy of fer-1, a specific inhibitor of ferroptosis, as a therapeutic agent for TBI in mice. The results from this study will advance our understanding of post-TBI cell death pathways and provide guidance for future preclinical TBI studies.

2 | METHODS

2.1 | Animals

The animal procedures used in this study were approved by the Animal Care and Experiment Committee of the School of Medicine, Shanghai Jiao Tong University. Male C57BL/6 mice (21-23 g) were housed for at least 7 days prior to surgery in a temperature (22-25°C) and humidity-controlled (50% relative humidity) animal facility with a 12-hour light/dark cycle. All mice were allowed free access to food and water except that food was withheld overnight before surgery. The whole experimental design is shown in Figure 1.

2.2 | CCI model and drug administration

In this study, surgical preparation and moderate CCI TBI was performed as previously described with only slight modification.[20,21] In brief, mice were anesthetized with sodium pentobarbital (70 mg/kg) and mounted in a stereotaxic frame (Stoelting, Varese, Italy). A sagittal incision was then made in the scalp and a circular craniotomy (4-mm diameter) was performed on the left side, midway between the bregma and the lambda with the medial edge 2 mm lateral to the midline. The bone flap was gently removed so that the underlying dura was not damaged. Prior to injury, a 3.0-mm rounded impacting tip was attached to an electromagnetically-controlled impacting device (PinPoint™ PCI3000 Precision Cortical Impactor™, Hatteras Instruments, Cary, USA) and the angle to the vertical plane was adjusted at 15°-20°, so that the tip was vertical to the dura. The mice were then subjected to moderate cortical contusion injury by a single impact (piston velocity: 3.0 m/s, deformation depth: 1.0 mm, dwell time: 180 ms). In the sham group, the mice received an identical procedure except for CCI injury. A total of 156 mice were subject to CCI injury and 40 to the sham operation. Nine mice were excluded because of death (CCI: 8/156; sham: 1/40). Thirty-two CCI mice were first labeled with the numbers "1,2,3.....31,32". Then, 32 successive numbers were randomly-selected from the random number table and the corresponding mice identified. Mice labeled with even numbers were assigned to the vehicle-treated group, while those labeled with odd numbers were assigned to the Fer-1-treated group.

Prior to drug administration, ferrostatin-1 (fer-1), a specific inhibitor of ferroptosis (Selleck, Houston, TX, USA) was diluted with 0.01% DMSO in saline to a final concentration of 1 mmol/L. Then, ferrostatin-1 (fer-1) and vehicle were labeled in a way that were blinded the investigators administering the drugs. The code was not

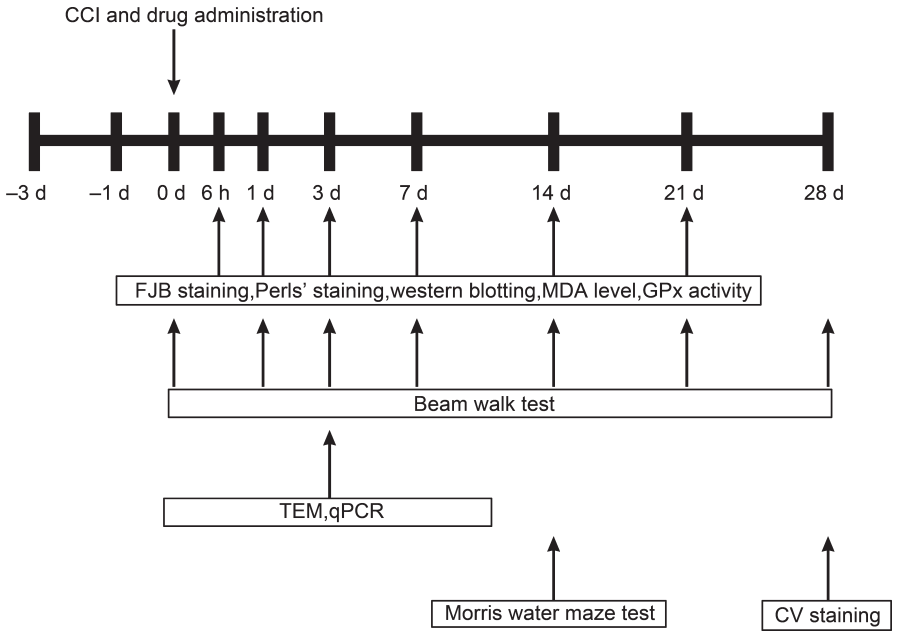

FIGURE 1 Experimental design. Chart illustrating our experimental design including controlled cortical impact (CCI), drug administration, FJB staining, Perl's staining, protein expression, lipid-reactive oxygen species (ROS), transmission electron microscopy (TEM), quantitative real-time PCR (qRT-PCR), neurobehavioral assessments and cresyl violet (CV) staining

revealed until the end of the study. Following CCI, 3 μL of ferrostatin-1 (1 mmol/L), or vehicle, was injected into the cerebral ventricle (coordinates: AP − 0.5 mm, lateral 1.0 mm, 2.5 mm beneath the pial surface) 30 minutes after injury. These dose and method of administration were based on previous studies.[12,22] The body temperature of the mice was maintained at 37°C during the entire procedure.

2.3 | Slice preparation

Mice were anesthetized with sodium pentobarbital (70 mg/kg intraperitoneally) and then trans-cardially perfused with 0.9% saline (4°C), followed by 4% paraformaldehyde (4°C). The brains were collected and post-fixed in 4% paraformaldehyde for 6 hours (h) at 4°C and then dehydrated in 20% and 30% sucrose solutions for 24 hours at 4°C successively. The brain tissues were then cut into consecutive coronal sections of 20 μm and stored at −80°C before use.

2.4 | Perl's staining

Cellular iron accumulation was detected by Perl's staining, as described previously with some modifications.[12,23] In brief, sections were immersed in distilled water for 3 minutes and then incubated in Perl's solution (5% potassium ferrocyanide [Sigma-Aldrich, St Louis, MO, USA]/5% hydrochloric acid) for 30 minutes, followed by washes in phosphate-buffered saline (PBS). Endogenous peroxidase activity was blocked with 0.3% hydrogen peroxide solution in methanol for 15 minutes, followed by three washes in PBS. Signals were developed by incubation for 2 minutes in 3,3-diaminobenzidine (DAB; Vector Laboratories, Burlingame, USA), and hematoxylin (Sigma-Aldrich, St Louis, MO, USA) was used for counterstaining. Cell counting was performed by an investigator who was blinded to the groups, as previously described (the regions of interest are shown in Figure 2A,B).[24] Briefly, iron-positive cells were quantified on stained sections at −0.7, −1.6, and −2.5 mm from the bregma. Three sections per animal were viewed and photographed under a microscope (Nikon TE300; Nikon). Iron-positive cells were calculated by four randomly-selected microscopic fields at × 200 magnification around the contusion area.

2.5 | Fluoro-Jade B (FJB) staining

Prior to staining, sections were mounted onto slides from distilled water and then air-dried for at least 30 minutes on a slide warmer at 50°C. Then, the tissue sections were immersed in a basic alcohol solution consisting of 1% sodium hydroxide in 80% ethanol for 5 minutes. They were then rinsed for 2 minutes in 70% ethanol, for 2 minutes in distilled water, and then incubated in 0.06% potassium permanganate solution for 10 minutes. Following a 1-2 minutes water rinse, the slides were then transferred for 10 minutes to a 0.0004% solution of Fluoro-Jade B (Millipore, Merck KGaA, Darmstadt, Germany) dissolved in 0.1% acetic acid vehicle. The slides were then rinsed three times in distilled water, ensuring that each rinse lasted 1 minute. Excess water was drained onto a paper towel, and the slides were then air-dried on a slide warmer at 50°C for at least 5 minutes. The air-dried slides were then cleared in xylene for at least 1 minute and then mounted with coverslips and DPX (Sigma) non-fluorescent mounting media. FJB-positive cells were quantified on stained sections at −0.7, −1.6, and −2.5 mm from the bregma. Three sections per animal were viewed and photographed under a microscope by a blinded observer. FJB-positive cells were calculated by four randomly-selected microscopic fields at × 200 magnification immediately adjacent to the lesion in three sections per animal. Cell degeneration counts were undertaken on a microscope (Nikon TE300; Nikon) using NIH Image J software (Bethesda, MD, USA).

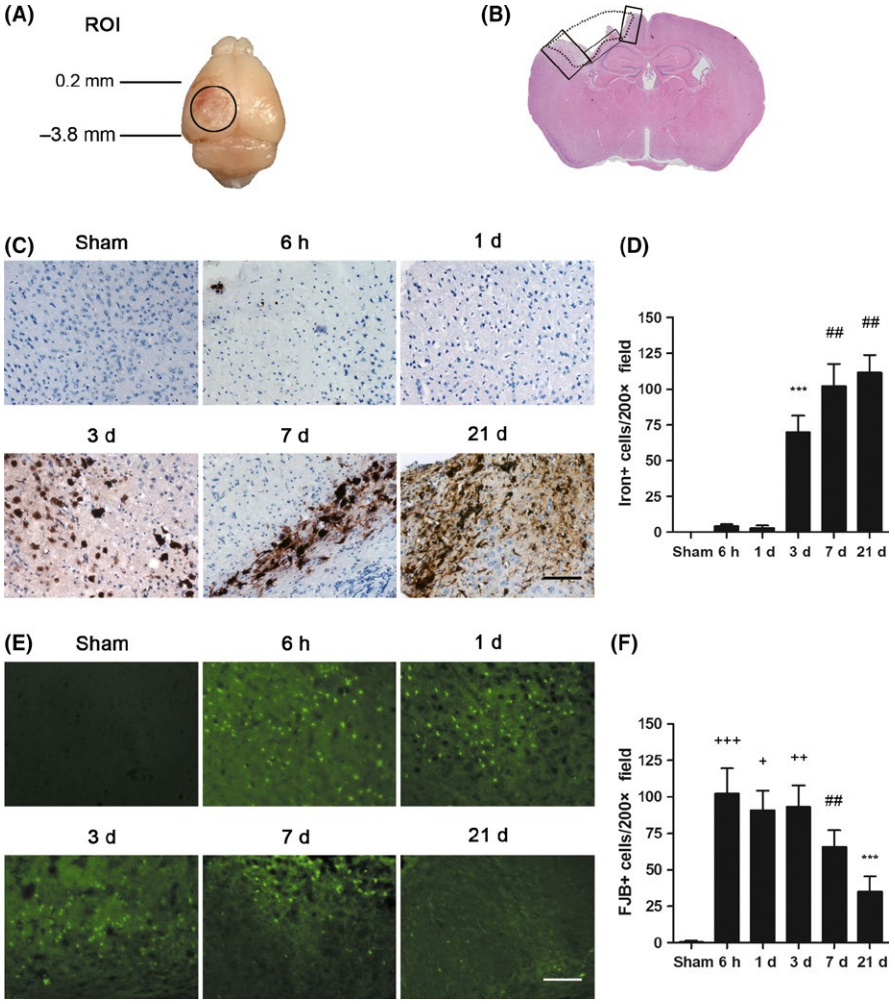

FIGURE 2 Features of neuronal degeneration and iron accumulation at different time points after controlled cortical impact (CCI) in mice. A, The region of interest (ROI) included tissue from 0.2 mm anterior to 3.8 mm posterior to the bregma. B, The cortical contusion area is denoted by the dotted box, and the regions of interest are depicted by rectangles. C, Field of interest and representative images of Perl's staining in brain sections at the indicated times after CCI. Scale bar: 50 μm. D, Quantification of iron-positive cells. Data are expressed as mean ± standard deviation (SD). Data were analyzed using analysis of variance (ANOVA) with Tukey's post hoc test. ***P < 0.001 vs the sham group, 6 h, 1 d; ##P < 0.01 vs 3 d (n = 6). E, Field of interest and representative images of Fluoro-Jade B (FJB) stained brain sections at the indicated times after controlled cortical impact injury (CCI). Scale bar: 50 μm. F, Quantification of FJB-positive cells. Data are expressed as mean ± SD. Data were analyzed using analysis of variance (ANOVA) with Tukey's post hoc test. +P < 0.05 vs 7 d; ++P < 0.01 vs 7 d; +++P < 0.001 vs 7 d; ##P < 0.01 vs 21 d; ***P < 0.001 vs sham group (n = 6)

2.6 | Western blotting

Mice were anesthetized with sodium pentobarbital (70 mg/kg intraperitoneally) and then perfused trans-cardially with 0.9% saline (4°C). Tissue samples of the ipsilateral cortex were dissected and homogenized in RIPA lysis buffer (Beyotime, Jiangsu, China) containing 1 mM phenylmethanesulfonyl fluoride (PMSF; Beyotime, Jiangsu, China). After sufficient lysis, the homogenate was centrifuged for 5 minutes at 4°C, supernatants were collected and total protein concentration was quantified using the BCA protein assay kit (Bio-Rad Laboratories, Hercules, CA, USA). Protein samples were separated on a 10% or 15% SDS-polyacrylamide gel by electrophoresis, according to molecular weight. Proteins were then electro-transferred onto polyvinylidene difluoride membranes (Millipore, Merck KGaA, Darmstadt, Germany), blocked with 5% skimmed milk at room temperature for 1 hour and then incubated with primary antibodies overnight at 4°C. After three washes in Tris-buffered saline with Tween 20 (TBST), for 5 minutes each, the membranes were incubated with secondary antibodies at room temperature for 2 hours. Signals were detected by chemiluminescence using ECL substrate (Pierce, Rockford, IL, USA). Band density was quantified by NIH Image J software (Bethesda, MD, USA) and data were normalized to GAPDH. The following primary antibodies were used: polyclonal rabbit anti-transferrin (1:3000, Abcam, Cambridge, UK); polyclonal rabbit anti-ferroportin (FPN; 1:2000, Abcam, Cambridge, UK); monoclonal rabbit anti-GPX4 (1:5000, Abcam, Cambridge, UK) and anti-GAPDH (1:1000, Cell Signaling Technology, Beverly, MA, USA).

2.7 | Quantitative real-time PCR

The mRNA levels of the ferroptosis-related genes ATP5G3, PTGS2, IREB2, CS, and RPL8 were analyzed in injured mice and sham controls at 3 days after TBI using quantitative real-time PCR (qRT-PCR). Briefly, total RNA was extracted from cortex tissue samples of the two groups (n = 5 each) using Trizol reagent (Invitrogen,Carlsbad, CA, USA) based on the manufacturer's protocol. The quantity of total RNA was determined using a NanoDrop ND-1000 (NanoDrop, Wilmington, DE). Reverse transcription to cDNA was achieved with PrimeScriptTM RT Master Mix (Perfect Real Time) (TakaraBio, Shiga, Japan). QRT-PCR was then conducted in a real-time PCR thermal cycler (Lightcycler System; Roche Diagnostics Corp., Indianapolis, IN, USA) using qPCR SYBR Green master mix (Yeasen, Shanghai, China). Glyceraldehyde 3-phosphate dehydrogenase (GAPDH) was used as an internal control to normalize the data. The primers are presented in Table 1.

TABLE 1 Sequences of primers used for qRT-PCR analysis of mRNA levels

Name	Sequence	Product size(bp)
GAPDH	Sense:5′ AGGTCGGTGTGAACGGATTTG 3′Antisense:5′ TGTAGACCATGTAGTTGAGGTCA 3′	129
ATP5G3	Sense:5′ GTGTGTCAGCTGATCCGAAG 3′Antisense:5′ AGGCAAATCCCAGGATAGCA 3′	214
PTGS2	Sense:5′ AATGTATGAGCACAGGATTTGACC 3′Antisense:5′ TGTCAGCACATATTTCATGATTAAACTTCG 3′	221
IREB2	Sense:5′ GTGACACTGTCTCTGTTCGT 3′Antisense:5′ TGTGTAACCATCCCACTGCC 3′	211
CS	Sense:5′ CATGCCAGTGCTTCTTCCACGA 3′Antisense:5′ CATGCCACCGTACATCATGTCC 3′	144
RPL8	Sense:5′ CGGGGTCCAAGAAGGTCATT 3′Antisense:5′ TGTACTTGTGGTAGGCACGG 3′	114

2.8 | Measurement of malondialdehyde (MDA) levels and glutathione peroxidase (GPx) activity

In order to determine lipid peroxide levels and evaluate GPx activity at different time points after TBI, we collected the ipsilateral cortex around the contusion area from the injury group, and the corresponding area from the sham group, and used commercially available kits to measure the MDA level and GPx activity (Beyotime, Jiangsu, China).

2.9 | Transmission electron microscopy (TEM)

Mice were perfused with 2% paraformaldehyde and 2% glutaraldehyde in 0.1 mol/L sodium cacodylate buffer. Brain samples, dissected from the margin of the lesion, were then post-fixed in phosphate-buffered glutaraldehyde (2.5%) and osmium tetroxide (1%). Brain samples were then cut and stained *en bloc* with 2% uranyl acetate (UA), dehydrated in acetone solutions at increasing concentrations, and embedded in an epoxy resin. Then, the sections (70-90 nm) were stained with lead citrate and uranyl acetate. Ultrastructural images were then captured with a transmission electron microscope (Hitachi HT7700, Japan).

2.10 | Morris water maze

The learning and memory functions of mice were evaluated 2 weeks after TBI with the Morris water maze, as previously described.[20,25] The maze was a round pool, which was 120 cm in diameter and 50 cm in depth. A white platform, 6 cm in diameter and 30 cm in height, lay in the southwest quadrant of the pool. The pool was filled with water and titanium dioxide was added in the water so that the water was white, and the platform was submerged 1 cm beneath the water surface. In each trial, a mouse was positioned facing the wall of the pool at one of four directions (east, south, west, and north) and then released to swim. Each trial was terminated once the mouse found the platform and rested on the platform for 10 seconds(s), or when the mouse did not discover the platform within the time limit of 60 seconds. The mouse was guided to the platform and allowed to rest on it for 10 seconds if it failed to find the platform. After each trial, the mice were placed in a dry cage. Each mouse was tested in four trials per day, for five consecutive days, with 4-minute intervals between trials. On the sixth day, each mouse was tested from one direction to assess cognitive function. The movement of each mouse was recorded by placing a video camera above the maze and the results, including latency, swimming speed, and swimming distance, were calculated using track analysis software (DigBehv, Jiliang Software Technology Company, Shanghai, China).

2.11 | Beam-walking test

Motor function of the mice was evaluated using the beam-walking test, as described previously.[26,27] The test was carried out on day 0 before CCI, and on days 1, 3, 7, 14, 21, and 28 post-TBI.

2.12 | Lesion volume assessment

To determine if the ferroptosis inhibitor, ferrostatin-1, attenuates tissue damage after CCI, we assessed lesion volume 21 days after TBI, with or without ferrostatin-1. Sections, 30 μm thick, were cut with a cryostat, starting at a point which was 0.2 mm anterior to the bregma. Serial sections, at 420 μm intervals, were then stained with cresyl violet (FD NeuroTechnologies, Columbia, MD, USA). Each section was measured for lesion area (mm^2) with NIH Image J software (Bethesda, MD, USA). Lesion volume was assessed in accordance with a previous report but with some modifications.[28] In brief, lesion volume was determined using the following equation, in which 'V' represents lesion volume (mm^3), 'A' stands for the lesion area (mm^2) and 'd' stands for the interval distance (in mm): $V = \{0.5A1 + 0.5(A1 + A2) + \ldots + 0.5(An - 1 + An) + 0.5An\}\, d$.

2.13 | Statistical analysis

Data are presented as means ± standard deviation (SD). Statistical analyses were carried out with SPSS 16.0. One-way analysis of variance (ANOVA) was used for comparisons within multiple groups. Tukey's post hoc test or Dunnett's post hoc test was used to determine specific differences between groups while the student's *t* test was used to compare mRNA level between sham and CCI or lesion volume between Fer1- and vehicle-treated mice after TBI. A *P* value less than 0.05 was considered to be statistically significant.

3 | RESULTS

3.1 | Intracellular iron content, and the number of degenerating neurons, were elevated in the injured cortex after TBI

At 6 hours and 1 day after injury, the TBI did not show significantly more iron deposition than the sham group. However, the number of iron-positive cells was significantly increased 3 days after TBI and continued to increase over time (3 days vs sham group $P < 0.001$;7, 21 vs 3 days $P < 0.01$; Figure 2C,D). During the same time-period, we also stained brain sections with FJB to evaluate neuron degeneration after TBI and found that the number of degenerating neurons around the lesion was significantly elevated at all time-points tested, but particularly at 6 hours, 1 and 3 days (6 hours vs 7 days $P < 0.001$; 1 day vs 7 days $P < 0.05$; 3 days vs 7 days $P < 0.01$; 7 days vs 21 days $P < 0.01$; 21 days vs sham group $P < 0.001$; Figure 2E,F).

3.2 | Iron metabolism dysfunction, upregulation of ferroptosis-related genes, lipid ROS accumulation and shrunken mitochondria were detected in the injured cortex after TBI

The peak expression of transferrin and FPN protein was detected 6 hours after TBI ($P < 0.001$ vs sham group; Figure 3A). Transferrin protein expression remained elevated at 1 and 3 days after TBI and returned to baseline on day 7. However, FPN protein returned to baseline on day 1 and was downregulated on day 21 (Figure 3A). We next assessed the mRNA levels of the ferroptosis-related genes ATP5G3, PTGS2, IREB2, CS and RPL8 in the cortex. As shown in Figure 3B,D after TBI, the mRNA levels of all these genes had increased significantly compared with the sham group (ATP5G3 $P < 0.01$; PTGS2 $P < 0.001$; IREB2 $P < 0.01$; CS $P < 0.05$; RPL8 $P < 0.05$). GPx4 protein expression was not significantly different when compared between the two groups of mice at any of the time-points tested (Figure 3C). However, GPx activity was significantly reduced at 6 hours ($P < 0.05$ vs sham group), 1 day ($P < 0.001$ vs sham group) and 3 days ($P < 0.001$ vs sham group) and returned to baseline on day 7 (Figure 3D). Lipid ROS level and MDA concentration was significantly elevated at 6 hours ($P < 0.01$ vs sham group), reached a peak on day 3 ($P < 0.001$ vs sham group) and returned to baseline on day 7 (Figure 3D).

Ultrathin sections from the margin of the injured cortex and the corresponding location in the sham mice at 3 days after the TBI or sham procedure was prepared, and obvious shrunken mitochondria in the soma of the TBI group was observed (Figure 3E).

3.3 | The intracerebroventricular administration of Fer-1 rescued iron accumulation, neuron degeneration and lesion volume after TBI

Three days after TBI, Fer-1–treated mice exhibited significantly fewer iron-positive cells than the vehicle-treated mice ($P < 0.05$; Figure 4A,B). In addition, Fer-1 administration significantly reduced neuronal death compared with vehicle treatment ($P < 0.01$; Figure 4C,D). Furthermore, treatment with Fer-1 significantly reduced the injury volume compared with that of the vehicle group at 3 days after TBI ($P < 0.01$; Figure 5A,B).

FIGURE 3 Iron metabolism dysfunction, the upregulation of ferroptosis-related genes, lipid-reactive oxygen species (ROS) accumulation and shrunken mitochondria were detected after traumatic brain injury in mice. Male C57BL/6 mice were sacrificed at the indicated time points after TBI. A, Western blot analysis for transferrin and ferroportin in the cortex at 6 h, 1 d,3 d, 7 d, and 3 weeks after injury (n = 6 each). Histogram shows the quantitative analysis of transferrin and ferroportin after TBI. Lane-loading differences were normalized by levels of GAPDH; Data are expressed as mean ± standard deviation (SD). Data were analyzed using analysis of variance (ANOVA) with Dunnett's post hoc test vs the sham group. *$P < 0.05$, ***$P < 0.001$ (n = 6 each). B, Total mRNA was extracted from the injured cortex, and quantitative real-time PCR was carried out with different primers. Glyceraldehyde 3-phosphate dehydrogenase (GAPDH) was used as an internal control to normalize the data, and results are shown as fold change of sham. Data are expressed as mean ± SD. Data were analyzed using the student's *t* test. *$P < 0.05$, **$P < 0.01$, ***Figure 6Ferrostatin-1 treatment attenuated TBI-induced deficits in motor and cognitive function. (A) Representative swimming tracks of the mice in all three groups on the sixth day of the Morris water maze test. B, The Morris water maze test showed that the latency and the swimming distance of the mice was significantly increased 2 weeks after TBI and that the administration of ferrostatin-1 significantly reduced the latency and swimming distance. However, there was no significant difference among the three groups in terms of swimming speed. Data are expressed as mean ± standard deviation (SD). Data were analyzed using analysis of variance (ANOVA) with Tukey's post hoc test (n = 10 each). ***$P < 0.001$ vs the sham group; ##$P < 0.01$ vs CCI+vehicle. C, Central administration of ferrostatin-1 improved motor function in the beam walk test. TBI-induced significant deficits in motor coordination compared with sham-injured mice and there were significant differences between the CCI+vehicle and the sham group at each time point. There was a significant difference between the CCI+Fer-1 group and the CCI+vehicle group at 14, 21, 28 d post-injury. Data are expressed as mean ± SD. Data were analyzed by ANOVA with Tukey's post hoc test (n = 10 each). ***$P < 0.001$ vs the sham group; #$P < 0.05$, ##$P < 0.01$ vs CCI+vehicle$P < 0.001$ (n = 5 each). C, Western blot analysis for GPX4 in the cortex at 6 h, 1 d, 3 d, 7 d, and 3 weeks after injury (n = 6 each). Histogram shows quantitative analysis of GPX4 after TBI. Lane-loading differences were normalized by levels of GAPDH. Data are expressed as mean ± SD. Data were analyzed using ANOVA with Dunnett's post hoc test vs the sham group (n = 6 each). D, GPX activity and MDA levels in the ipsilateral cortex at the indicated times after TBI. Data are expressed as mean ± SD. Data were analyzed using ANOVA with Dunnett's post hoc test vs the sham group. *$P < 0.05$, **$P < 0.01$, ***$P < 0.001$ (n = 6 each). E, Ultrastructure of the ipsilateral cortex 3 d after CCI in mice. Male C57BL/6 mice were sacrificed 3 d after TBI or sham operation (n = 3 each). The ultrastructure of the ipsilateral cortex was captured by transmission electron microscopy. Red arrowheads indicate shrunken mitochondria. Histogram showed mitochondrial area frequency in neurons of the ipsilateral cortex. Number of mitochondria, sham: n = 216; CCI: n = 342. Black arrows indicate increased frequency of shrunken mitochondria in CCI groups. Scale bars: upper panel, 2 μm and bottom panel, 500 nm

3.4 | Treatment with Fer-1 ameliorated TBI-induced deficits in cognitive and motor function

The Morris water maze test showed that the latency (45.5 ± 3.1 s vs 13.7 ± 2.4 s, respectively) and swimming distance (7909 ± 647 mm vs 2522 ± 507 mm, respectively) of the vehicle-treated-TBI mice were significantly increased compared with the sham group at 6 days ($P < 0.001$; Figure 6A,B), showing obvious learning and cognitive defects after TBI. Furthermore, compared with corresponding values in the vehicle-treated mice, the latency and swimming distance of the Fer-1-treated mice were significantly ameliorated (latency: 45.5 ± 3.1 vs 27.9 ± 4.2 s, respectively, $P < 0.01$; swimming distance: 7909 ± 647 mm vs 4402 ± 654 mm, respectively, $P < 0.01$; Figure 6A,B). The beam walk test showed significant differences between the sham and the two TBI groups at all time-points post-injury ($P < 0.001$; Figure 6C). Notably, treatment with the ferroptosis

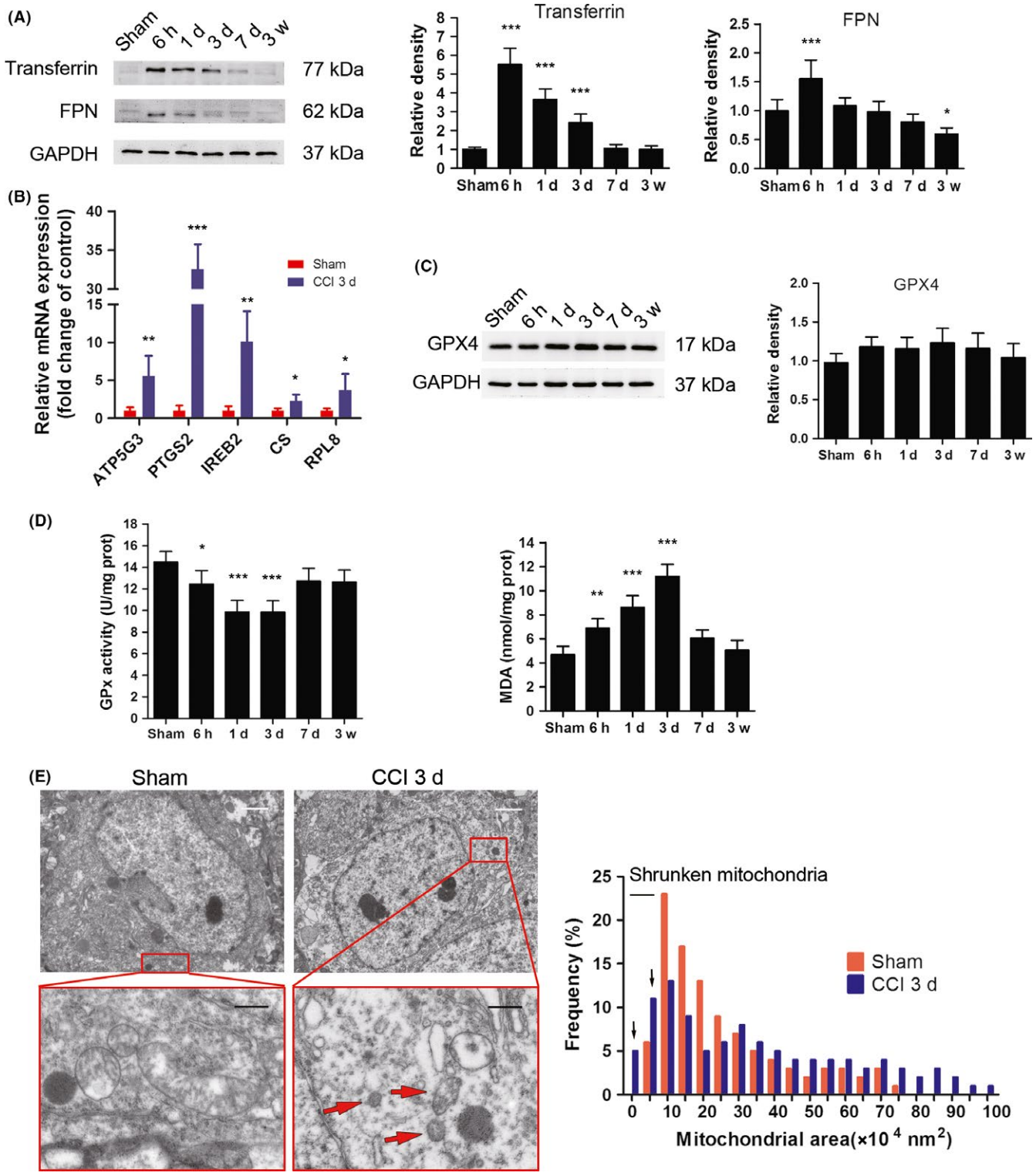

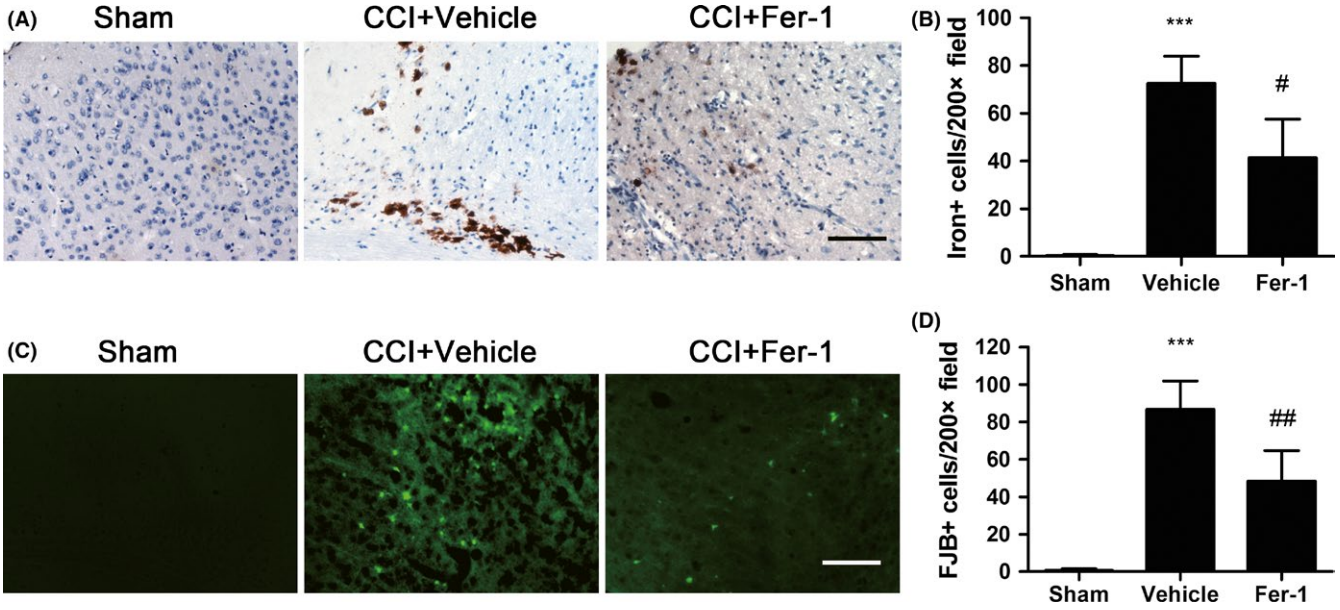

FIGURE 4 Ferrostatin-1 treatment attenuated neuronal degeneration and iron accumulation after TBI. Mice were sacrificed 3 d after TBI. The brains of Sham, CCI+Vehicle and CCI+ Ferrostatin-1(Fer-1) groups were obtained. A, Field of interest and representative images of Perl's staining in brain sections. B, Quantification of iron-positive cells. Data are expressed as mean ± standard deviation (SD). Data were analyzed using analysis of variance (ANOVA) with Tukey's post hoc test. ***P < 0.001 vs sham group, #P < 0.05 vs CCI+Vehicle (n = 6 each). C, Field of interest and representative images of Fluoro-Jade B (FJB) stained brain sections. D, Quantification of FJB-positive cells. Data are expressed as mean ± SD. Data were analyzed using ANOVA with Tukey's post hoc test. ***P < 0.001 vs the sham group, ##P < 0.01 vs CCI+Vehicle (n = 6 each). Scale bars: 50 μm (A and C)

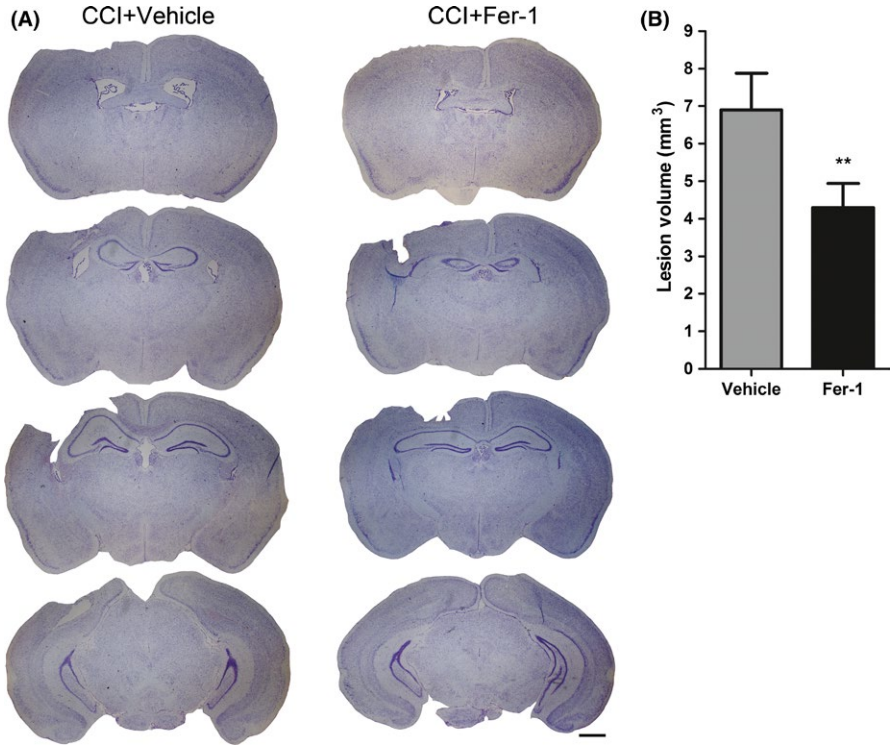

FIGURE 5 Ferrostatin-1 treatment reduced lesion volume after TBI. Mice were sacrificed 28 d after TBI. The brains of Sham, CCI+Vehicle and CCI+ Ferrostatin-1 (Fer-1) mice were obtained and sections of the samples were stained with cresyl violet. A, Representative images from each group are shown. Scale bars: 1 mm. B, Central administration of ferrostatin-1 significantly reduced lesion volume compared with the CCI+vehicle group (**P < 0.01). Data are expressed as mean ± standard deviation (SD). Student's t test, n = 5

specific inhibitor, Fer-1, significantly reduced right hind foot faults only on day 14, 21 and 28 post-TBI (14 days, 28 days P < 0.05; 21 days P < 0.01; Figure 6C) when compared with the vehicle-treated TBI group.

4 | DISCUSSION

Ferroptosis is a newly discovered form of regulated cell death that plays a major role in various diseases, including tumor, stoke, cold

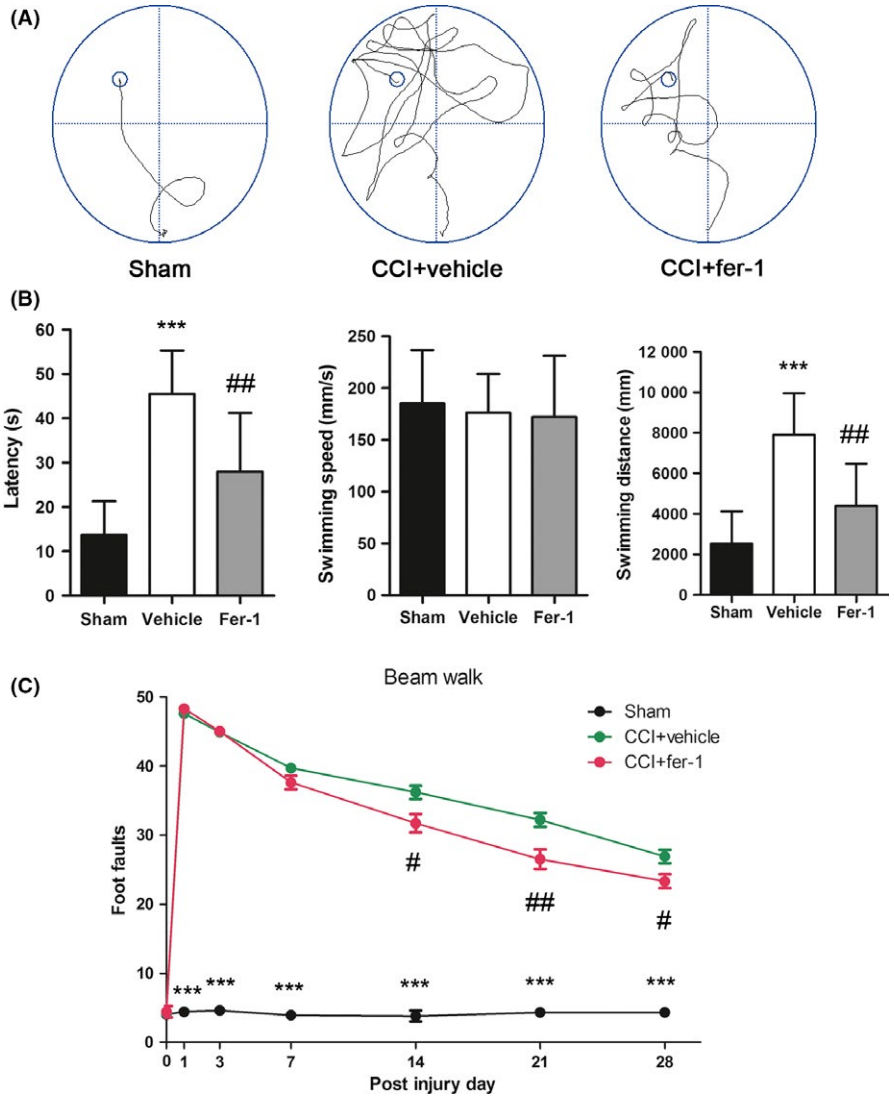

FIGURE 6 Ferrostatin-1 treatment attenuated TBI-induced deficits in motor and cognitive function. (A) Representative swimming tracks of the mice in all three groups on the sixth day of the Morris water maze test. B, The Morris water maze test showed that the latency and the swimming distance of the mice was significantly increased 2 weeks after TBI and that the administration of ferrostatin-1 significantly reduced the latency and swimming distance. However, there was no significant difference among the three groups in terms of swimming speed. Data are expressed as mean ± standard deviation (SD). Data were analyzed using analysis of variance (ANOVA) with Tukey's post hoc test (n = 10 each). ***P < 0.001 vs the sham group; ##P < 0.01 vs CCI+vehicle. C, Central administration of ferrostatin-1 improved motor function in the beam walk test. TBI-induced significant deficits in motor coordination compared with sham-injured mice and there were significant differences between the CCI+vehicle and the sham group at each time point. There was a significant difference between the CCI+Fer-1 group and the CCI+vehicle group at 14, 21, 28 d post-injury. Data are expressed as mean ± SD. Data were analyzed by ANOVA with Tukey's post hoc test (n = 10 each). ***P < 0.001 vs the sham group; #P < 0.05, ##P < 0.01 vs CCI+vehicle

stress, acute kidney failure, and neural degeneration.[13,18,29-32] As in TBI, a recent study reported that ferroptotic death possibly occurs at early time points after TBI in the pediatric rat CCI model due to elevated levels of 15-HpETE-PE in the brain cortex and hippocampus, along with increased expression of 15LO2 and decreased levels of GPX4.[19] However, the precise role of ferroptosis in adult rodents remains unknown. In the present study, using an adult mouse CCI model, we found that iron and lipid ROS accumulated significantly after TBI, along with iron metabolism dysfunction, the upregulation of ferroptosis-related genes and the reduced activity of GPx. In addition, using TEM, we identified shrunken mitochondria in the soma of neurons 3 days after TBI. Furthermore, administration of the ferroptosis specific inhibitor, Fer-1, not only reduced iron accumulation and neural death but also ameliorated TBI-induced deficits in cognitive and motor function. Taken together, these findings suggested that ferroptosis occurs in the adult mouse CCI model and might thus represent a potential therapeutic target for TBI patients.

One of the typical characteristics of ferroptosis is iron accumulation. Evidence indicates that chronic TBI patients might show an abnormally high accumulation of iron, which is positively related to cognitive impairment.[33] This phenomenon is consistent with our

observation of iron accumulation around the injury lesion at 3 days or longer after CCI. In additional, our results showed a temporal profile of intracellular iron level changes over time. Iron deposits started to increase on day 3 and continued to elevate over time within 21 days after TBI. To study the mechanisms underlying iron accumulation, we investigated the expression levels of two iron metabolism proteins, transferrin, and FPN. A previous study showed that transferrin, which transports iron into cells, is essential for the induction of ferroptosis, and that experiments involving the knock down of transferrin resulted in reduced cell death and lipid ROS accumulation.[34,35] Moreover, FPN, which is responsible for the removal of iron from cells, was downregulated in breast cancer cells and underwent ferropotosis. The overexpression of FPN resulted in reduced ROS and cell death whereas knockdown of FPN promoted cell death following treatment with siramesine and lapatinib.[35] It is noteworthy that in our present study, Western blotting showed that the expression level of transferrin and FPN were both significantly elevated at 6 hours after TBI, thus explaining why iron deposits were not elevated at early time points. The expression of FPN fell to baseline on day 1 and was reduced on day 21. However, the upregulated expression of transferrin lasted until day 3. This finding is compatible with the phenomenon that iron accumulation started on day 3 after TBI.

Another characteristic of ferroptosis is lipid ROS accumulation. Numerous studies have suggested that GPX4, which is responsible for catalyzing the reduction in lipid peroxides, is a key regulator of ferroptosis.[36-39] Previous research has claimed that both GPX4 expression and GPx activity was reduced after TBI, and that therefore, the expression of 15LO2 was elevated during the early time points in pediatric rats.[19] Other investigations have reported the activity of GPx to be reduced after acute brain injuries in adult mice, including TBI and hemorrhage stroke.[12,40] Our present study showed that GPx activity was decreased, and MDA levels elevated, within 3 days of TBI. However, the downregulated expression level of GPX4 was not observed at all time points. The reasons underlying this difference might include different ages and species of the mice used, as our study used adult mice instead of pediatric rats.

Cell death, one of the essential mechanisms for maintaining tissue homeostasis throughout life, plays a critical role in brain tissue damage, along with the behavior and memory function impairment after acute brain injury. In general, necroptosis tends to occur 6 hours after TBI, while apoptosis occurs within 3 days.[7,8] In the present study, we also found that neuronal degeneration mainly occurred within 3 days, and lasted until 21 days post-TBI. Three days after TBI, we observed shrunken mitochondria around the brain injury lesions using TEM, thus providing powerful evidence for the occurrence of ferroptosis after TBI. As far as we know, this is the first study to observe shrunken mitochondria in a TBI animal model.[10,12] Furthermore, other forms of cell death, including necrosis, autophagy, and apoptosis, were also observed in the injured brain, suggesting that brain tissue damage may represent a combination of several different forms of cell death.[7,41]

Fer-1 has previously been identified as a potent and specific inhibitor of ferroptosis.[10] Moreover, studies have shown that Fer-1 inhibited cell death in various cellular disease models such as Huntington's disease (HD), acute brain injury, periventricular leukomalacia (PVL), and kidney failure.[42] Other studies have shown that Fer-1 reduced glutamate-induced ferroptosis in organo-typical hippocampal slices, and inhibited ferroptosis-related to stroke and Parkinson's disease in animal models.[18,22,32,43] In our current study, there was a reduction in iron accumulation and attenuated neuronal degeneration in TBI animals which had been treated with Fer-1. In addition, using the Morris water maze test and the beam-walking test, we found that Fer-1 also ameliorated TBI-induced impairments in cognitive and motor function. However, in the present study, we administrated Fer-1 by cerebral ventricle injection, which is not a feasible drug-delivery method for clinical scenarios. Consequently, the efficacy of a range of clinically-feasible drug-delivery methods needs to be tested in future studies, including intraperitoneal or intravenous delivery.

In conclusion, our data provided significant evidence to confirm the presence of ferroptosis in an animal model of TBI, including iron accumulation, elevated expression of transferrin, reduced activity of GPx, lipid ROS accumulation, and shrunken mitochondria. Furthermore, treatment with Fer-1 reduced neuronal cell death and improved long-term cognitive and motor function. Thus, these findings demonstrated a new form of cell death in TBI and provide a novel therapeutic target for protecting the injured brain. Further studies are now needed to determine the therapeutic window of Fer-1 and develop clinically-feasible drugs.

ACKNOWLEDGMENTS

This work was partly supported by Doctoral Innovation Fund Projects from Shanghai Jiao Tong University School of Medicine (BXJ201824) and partly supported by National Natural Science Foundation of China (No. 81772058, 81471856, 81471244 and 81771317).

CONFLICT OF INTEREST

The authors declare no conflict of interest.

ORCID

Bao-Shu Xie http://orcid.org/0000-0002-0684-5341

REFERENCES

1. Brazinova A, Rehorcikova V, Taylor MS, et al. Epidemiology of traumatic brain injury in europe: a living systematic review. *J Neurotrauma*. 2016;33:1-30.
2. Majdan M, Plancikova D, Maas A, et al. Years of life lost due to traumatic brain injury in Europe: a cross-sectional analysis of 16 countries. *PLoS Med*. 2017;14:e1002331.
3. Abou-Abbass H., Bahmad H., Ghandour H., et al. Epidemiology and clinical characteristics of traumatic brain injury in Lebanon: a systematic review. *Medicine (Baltimore)* 2016;95:e5342.
4. Potts M. B., Koh S. E., Whetstone W. D., et al. Traumatic injury to the immature brain: inflammation, oxidative injury, and

iron-mediated damage as potential therapeutic targets. *NeuroRx* 2006;3:143-153.
5. McGinn MJ, Povlishock JT. Pathophysiology of traumatic brain injury. *Neurosurg Clin N Am*. 2016;27:397-407.
6. Al Nimer F, Beyeen AD, Lindblom R, et al. Both MHC and non-MHC genes regulate inflammation and T-cell response after traumatic brain injury. *Brain Behav Immun*. 2011;25:981-990.
7. Liu T., Zhao D. X., Cui H., et al. Therapeutic hypothermia attenuates tissue damage and cytokine expression after traumatic brain injury by inhibiting necroptosis in the rat. *Sci Rep* 2016;6:24547.
8. Jia F, Mao Q, Liang YM, Jiang JY. Effect of post-traumatic mild hypothermia on hippocampal cell death after traumatic brain injury in rats. *J Neurotrauma*. 2009;26:243-252.
9. Adamczak SE, de Rivero Vaccari JP, Dale G, et al. Pyroptotic neuronal cell death mediated by the AIM2 inflammasome. *J Cereb Blood Flow Metab*. 2014;34:621-629.
10. Dixon SJ, Lemberg KM, Lamprecht MR, et al. Ferroptosis: an iron-dependent form of nonapoptotic cell death. *Cell*. 2012;149:1060-1072.
11. Lachaier E, Louandre C, Godin C, et al. Sorafenib induces ferroptosis in human cancer cell lines originating from different solid tumors. *Anticancer Res*. 2014;34:6417-6422.
12. Li Q, Han X, Lan X, et al. Inhibition of neuronal ferroptosis protects hemorrhagic brain.*JCI*. *Insight*. 2017;2:e90777.
13. Tuo QZ, Lei P, Jackman KA, et al. Tau-mediated iron export prevents ferroptotic damage after ischemic stroke. *Mol Psychiatry*. 2017;22:1520-1530.
14. Martin-Sanchez D, Ruiz-Andres O, Poveda J, et al. Ferroptosis, but not necroptosis, is important in nephrotoxic folic acid-induced AKI. *J Am Soc Nephrol*. 2017;28:218-229.
15. Stockwell BR, Friedmann Angeli JP, Bayir H, et al. Ferroptosis: a regulated cell death nexus linking metabolism, redox biology, and disease. *Cell*. 2017;171:273-285.
16. Doll S, Proneth B, Tyurina YY, et al. ACSL4 dictates ferroptosis sensitivity by shaping cellular lipid composition. *Nat Chem Biol*. 2017;13:91-98.
17. Sheng X, Shan C, Liu J, Yang J, Sun B, Chen D. Theoretical insights into the mechanism of ferroptosis suppression via inactivation of a lipid peroxide radical by liproxstatin-1. *Phys Chem Chem Phys*. 2017;19:13153-13159.
18. Zille M, Karuppagounder SS, Chen Y, et al. Neuronal death after hemorrhagic stroke in vitro and in vivo shares features of ferroptosis and necroptosis. *Stroke*. 2017;48:1033-1043.
19. Wenzel SE, Tyurina YY, Zhao J, et al. PEBP1 wardens ferroptosis by enabling lipoxygenase generation of lipid death signals. *Cell*. 2017;171(628–641):e26.
20. Wang CF, Zhao CC, Jiang G, Gu X, Feng JF, Jiang JY. The role of post-traumatic hypothermia in preventing dendrite degeneration and spine loss after severe traumatic brain injury. *Sci Rep*. 2016;6:37063.
21. Lee S, Mattingly A, Lin A, et al. A novel antagonist of p75NTR reduces peripheral expansion and CNS trafficking of pro-inflammatory monocytes and spares function after traumatic brain injury. *J Neuroinflammation*. 2016;13:88.
22. Van Do B, Gouel F, Jonneaux A, et al. Ferroptosis, a newly characterized form of cell death in Parkinson's disease that is regulated by PKC. *Neurobiol Dis*. 2016;94:169-178.
23. Wu H, Wu T, Xu X, Wang J, Wang J. Iron toxicity in mice with collagenase-induced intracerebral hemorrhage. *J Cereb Blood Flow Metab*. 2011;31:1243-1250.
24. Chang C. F., Cho S., Wang J. (-)-Epicatechin protects hemorrhagic brain via synergistic Nrf2 pathways. *Ann Clin Transl Neurol* 2014;1:258-271.
25. Lin Y, Wan JQ, Gao GY, et al. Direct hippocampal injection of pseudo lentivirus-delivered nerve growth factor gene rescues the damaged cognitive function after traumatic brain injury in the rat. *Biomaterials*. 2015;69:148-157.
26. Fox GB, Fan L, Levasseur RA, Faden AI. Sustained sensory/motor and cognitive deficits with neuronal apoptosis following controlled cortical impact brain injury in the mouse. *J Neurotrauma*. 1998;15:599-614.
27. Sabirzhanov B, Stoica BA, Zhao Z, et al. miR-711 upregulation induces neuronal cell death after traumatic brain injury. *Cell Death Differ*. 2016;23:654-668.
28. Dash PK, Orsi SA, Zhang M, et al. Valproate administered after traumatic brain injury provides neuroprotection and improves cognitive function in rats. *PLoS ONE*. 2010;5:e11383.
29. Zhu S, Zhang Q, Sun X, et al. HSPA5 regulates ferroptotic cell death in cancer cells. *Cancer Res*. 2017;77:2064-2077.
30. Muller T, Dewitz C, Schmitz J, et al. Necroptosis and ferroptosis are alternative cell death pathways that operate in acute kidney failure. *Cell Mol Life Sci*. 2017;74:3631-3645.
31. Hattori K, Ishikawa H, Sakauchi C, Takayanagi S, Naguro I, Ichijo H. Cold stress-induced ferroptosis involves the ASK1-p38 pathway. *EMBO Rep*. 2017;18:2067-2078.
32. Guiney SJ, Adlard PA, Bush AI, Finkelstein DI, Ayton S. Ferroptosis and cell death mechanisms in Parkinson's disease. *Neurochem Int*. 2017;104:34-48.
33. Lu L, Cao H, Wei X, Li Y, Li W. Iron deposition is positively related to cognitive impairment in patients with chronic mild traumatic brain injury: assessment with susceptibility weighted imaging. *Biomed Res Int*. 2015;2015:470676.
34. Gao M, Monian P, Quadri N, Ramasamy R, Jiang X. Glutaminolysis and transferrin regulate ferroptosis. *Mol Cell*. 2015;59:298-308.
35. Ma S, Henson ES, Chen Y, Gibson SB. Ferroptosis is induced following siramesine and lapatinib treatment of breast cancer cells. *Cell Death Dis*. 2016;7:e2307.
36. Yang WS, SriRamaratnam R, Welsch ME, et al. Regulation of ferroptotic cancer cell death by GPX4. *Cell*. 2014;156:317-331.
37. Friedmann Angeli JP, Schneider M, Proneth B, et al. Inactivation of the ferroptosis regulator Gpx4 triggers acute renal failure in mice. *Nat Cell Biol*. 2014;16:1180-1191.
38. Imai H, Matsuoka M, Kumagai T, Sakamoto T, Koumura T. Lipid peroxidation-dependent cell death regulated by GPx4 and ferroptosis. *Curr Top Microbiol Immunol*. 2017;403:143-170.
39. Maiorino M, Conrad M, Ursini F. GPx4, Lipid Peroxidation, and Cell Death: discoveries, Rediscoveries, and Open Issues. *Antioxid Redox Signal*. 2018;29:61-74.
40. Cao Y, Gao Y, Xu S, et al. Glutamate carboxypeptidase II gene knockout attenuates oxidative stress and cortical apoptosis after traumatic brain injury. *BMC Neurosci*. 2016;17:15.
41. Jin Y, Lin Y, Feng JF, Jia F, Gao GY, Jiang JY. Moderate hypothermia significantly decreases hippocampal cell death involving autophagy pathway after moderate traumatic brain injury. *J Neurotrauma*. 2015;32:1090-1100.
42. Skouta R, Dixon SJ, Wang J, et al. Ferrostatins inhibit oxidative lipid damage and cell death in diverse disease models. *J Am Chem Soc*. 2014;136:4551-4556.
43. Speer RE, Karuppagounder SS, Basso M, et al. Hypoxia-inducible factor prolyl hydroxylases as targets for neuroprotection by "antioxidant" metal chelators: from ferroptosis to stroke. *Free Radic Biol Med*. 2013;62:26-36.

How to cite this article: Xie B-S, Wang Y-Q, Lin Y, et al. Inhibition of ferroptosis attenuates tissue damage and improves long-term outcomes after traumatic brain injury in mice. *CNS Neurosci Ther*. 2019;25:465–475. https://doi.org/10.1111/cns.13069